# Brittle deformation and damage-induced seismic wave anisotropy in rocks

Y. Hamiel,[1] V. Lyakhovsky,[1] S. Stanchits,[2] G. Dresen[2] and Y. Ben-Zion[3]

[1]*Geological Survey of Israel, 30 Malkhei Israel St., 95501, Jerusalem, Israel. E-mail: yariv@gsi.gov.il*
[2]*Geo Forschungs Zentrum Potsdam, Telegrafenberg D420, 14473, Potsdam, Germany*
[3]*Department of Earth Sciences, USC, Los Angeles, CA 90089–0740, USA*

## SUMMARY

We study the relations between rock fracturing, non-linear deformation and damage- and stress-induced anisotropy of seismic waves by comparing theoretical predictions of a damage rheology model to results of laboratory experiments with granite samples. The employed damage model provides a generalization of Hookean elasticity to a non-linear continuum mechanics framework of cracked media incorporating degradation and recovery of the effective elastic properties, along with gradual accumulation of irreversible deformation beyond the elastic regime. The model assumes isotropic distribution of local microcracks expressed in terms of a scalar damage variable, but the non-linear elastic response caused by the opening, closure and evolution of the internal cracks is predicted to lead to seismic wave anisotropy. We develop relations between the seismic wave anisotropy, internal rock damage and stress field, and test the viscoelastic damage rheology against sets of laboratory experiments with cylindrical granite samples. The observed data include measurements of stress and strain in three loading cycles culminating in a final macroscopic failure, together with measured wave velocities along and perpendicular to the axis of the cylinder. Using a single set of parameters, the model fits well the overall evolution of the axial and transversal stress–strain relations, as well as the anisotropic elastic wave velocities, during all cycles from the onset of fracturing in the first cycle until the macroscopic failure in the final cycle.

**Key words:** Elasticity and anelasticity; Fault zone rheology; Seismic anisotropy; Dynamics and mechanics of faulting, Fractures and faults; Rheology: crust and lithosphere.

## 1 INTRODUCTION

Crustal rocks are often treated as isotropic and linear elastic material with constant elastic wave velocities. This assumption might be appropriate for rocks with relatively low damage, associated with internal distributions of cracks and voids, under relatively low loads. However, rocks subjected to sufficiently high loads develop internal damage and exhibit clear deviations from linear elasticity (e.g. Jaeger & Cook 1979). In particular, laboratory fracturing experiments indicate that changes in the effective elastic moduli become very significant, and the internal rock damage localizes in the final stages before macroscopic brittle failure (e.g. Mogi 1962; Lockner & Byerlee 1980; Lockner *et al.* 1992). One basic manifestation of damaged rocks is crack-induced anisotropy of elastic waves, which depends on the crack density and applied stress level. This has been measured in the laboratory for many rock types (e.g. Nur & Simmons 1969; Nur 1971; Bonner 1974; Lockner *et al.* 1977; Sammonds *et al.* 1989; Sayers *et al.* 1990; Zamora & Poirier 1990; Stanchits *et al.* 2006; Hall *et al.* 2008) and is also seen in the vicinity of large active fault zones and other environments with high rock damage (e.g. Crampin 1987; Leary *et al.* 1990; Miller & Savage 2001; Peng & Ben-Zion 2004; Liu *et al.* 2005; Boness & Zoback 2006).

Stress–strain relations of a damaged rock are usually approximated by an elastic body with cracks or inclusions embedded inside an otherwise homogeneous matrix. For example, the elastic field of ellipsoidal inclusions (Eshelby 1957) allows the construction of a model for a material with cracks. This approach was successfully applied to synthetic materials with known crack geometries and matrix elastic parameters (e.g. Christensen 1979; Rathore *et al.* 1995). A useful related framework is the self-consistent model of O'Connell & Budiansky (1974) and Budiansky & O'Connell (1976) for materials with random crack distributions. The averaging of random crack orientations yields effective moduli that depend on crack densities but do not depend on crack orientations. Another method utilizes the crack-density tensor for finding the effective properties of a solid with arbitrary crack interactions (e.g. Kachanov 1980, 1992; Sayers & Kachanov 1991, 1995). These two approaches were used by several researchers to study effects of crack- and stress-induced anisotropy on seismic wave propagation (e.g. Hudson 1981;

GJI Seismology

Schoenberg & Douma 1988; Schoenberg & Sayers 1995; Chapman 2003; Verdon *et al.* 2008). Following the tensorial damage approach, Sayers (2002) expressed the effective elastic moduli in terms of second and fourth rank crack-density tensors and presented an inversion strategy for reconstructing the damage tensor from measured anisotropy of elastic waves. Such inversion leads to relations between the measured wave velocities and crack-density tensor (e.g. Schubnel & Gueguen 2003; Stanchits *et al.* 2006; Hall *et al.* 2008). These approaches assume elastic crack opening and closure, with instantaneous material degradation and recovery, and they do not account for gradual and permanent changes of damage with ongoing loading.

In the framework of continuum mechanics, to simulate the observed degradation of the effective elastic properties, a non-dimensional scalar or tensor damage variable is introduced in damage rheology models. The damage state variable characterizes a properly chosen volume of rock, so that the density of the internal flaws (e.g. microcracks in a laboratory specimen or small faults in the Earth's crust) within this volume may be considered uniform. Following theoretical developments (e.g. Kachanov 1986; Chaboche 1988; Rabotnov 1988; Lemaitre 1996) in the framework of continuum damage mechanics, Hansen & Schreyer (1994) demonstrated that predictions of a linear scalar damage model correlate well with changes of the Young's modulus but not with changes of the apparent Poisson's ratio. For this reason, Ju (1990) and Hansen & Schreyer (1994) suggested to upgrade the damage variable from a scalar to a tensor quantity. Such linear tensorial damage models contain at least three adjustable parameters that can be used to simulate the evolution of the apparent Poisson's ratio (see review of Kachanov 1994). Although the linear tensorial damage models are capable of reproducing damage accumulation, they do not attempt to describe healing and material recovery under 3-D compaction. The local entropy production by damage and healing processes is the product of the thermodynamic force related to the damage/healing and the damage/healing rate (e.g. Lyakhovsky *et al.* 1997a, 1997b; Hamiel *et al.* 2004b). Hence, healing under 3-D compaction in the linear scalar and linear tensorial damage models is prohibited by the second law of thermodynamics, since it leads to negative entropy production. This limits the applicability of these models to long-term geological processes that should account for both rock degradation and recovery.

Variations of Young's modulus and Poisson's ratio with damage intensity under different types of load can be described using a nonlinear damage model, where the free energy of an elastic solid is augmented by an additional non-linear term, and the evolving elastic moduli are connected to a single scalar damage variable (e.g. Lyakhovsky & Myasnikov 1984, 1985; Lyakhovsky *et al.* 1997a, 1997b; Hamiel *et al.* 2004a,b; Lyakhovsky & Ben-Zion 2008). A brief background material with the main features of this damage model is presented in Section 3. Myasnikov & Topale (1987) derived asymptotic dispersion relations for the velocity of seismic waves propagating in an arbitrary direction in the non-linear elastic model, with the additional second-order energy term and small values of the damage parameter. Lyakhovsky & Myasnikov (1987, 1988) demonstrated that stress-induced seismic wave anisotropy in rocks with low damage is compatible with field observations, and that the predicted stress-induced velocity variations have considerable effects on seismic ray tracing.

Modelling the observed stress- and damage-induced seismic anisotropy requires dispersion relations for an arbitrary level of damage. In this paper, we derive analytical expressions for velocities of direct seismic waves as a function of damage and strain

(Section 4) and apply our damage model to laboratory experiments with Aue granite samples (Section 5). The measured quantities are axial and transverse components of stress–strain curves for three consecutive loading cycles and vertical and horizontal wave velocities. We first calibrate the damage-rheology model parameters using the measured stress–strain data. Then we calculate the velocities for *P* waves propagating in the axial and transversal directions and compare the results with the laboratory measured values. We show that the employed damage rheology model can quantitatively account for the main stages of the quasi-static deformation and also reproduce damage- and stress-induced seismic wave anisotropy measured during each cycle of the laboratory experiments.

## 2 EXPERIMENTAL SETTING AND RESULTS

The experiments were performed on cylindrical granite sample from Aue, Germany, of 50 mm diameter and 100 mm length. The experimental setup has been described in detail in Stanchits *et al.* (2006). The mineral composition of the Aue granite contains 30 per cent quartz, 40 per cent plagioclase, 20 per cent potassium feldspar and 10 per cent mica; the grain sizes range from 0.9 to 1.8 mm, with an average value of 1.3 mm (Zang *et al.* 2000). To monitor strain, two pairs of orthogonally oriented strain gauges were glued onto the cylindrical sample surface. Acoustic emission (AE) activity and ultrasonic velocity changes were monitored by 12 *P*- and eight *S*-wave piezoelectric sensors; the wave velocities were measured parallel and normal to the loading direction every 30–40 s (Stanchits *et al.* 2006). The full-waveform AE data and ultrasonic signals for the wave velocity measurements were stored in a 12-channel transient recording system (PRÖKEL, Germany), with an amplitude resolution of 16 bit at 10 MHz sampling rate.

The granite sample was subjected to two types of loading. First, hydrostatic pressure $\sigma_1 = \sigma_2 = \sigma_3$ was increased up to 120 MPa and then decreased down to 60 MPa (Stanchits *et al.* 2006). Subsequently, the sample was subjected to increasing axial stress in three consecutive cycles at confining pressures of 60, 40 and 20 MPa. The first two cycles were interrupted when differential stresses reached about 450 MPa and axial strains were between 0.7 and 0.8 per cent. During the third cycle, the loading process was carried out until catastrophic failure of the sample (Fig. 1). At all confining pressures the experimental results show significant stress-induced *P*-wave velocity anisotropy. In general, the axial *P* velocities are higher than the transverse velocities (up to about 40 per cent), and the *P*-wave anisotropy increases with increasing axial loading and with increasing proximity to the total macroscopic failure (Stanchits *et al.* 2006). Toward the macroscopic failure in the third loading cycle, the strong increase of anisotropy is likely due to strong localized deformation. The observed *S*-wave velocity variations are relatively small, up to only 6 per cent, not well resolved and not analysed in this study. In the current paper only the axial loading cycles following the earlier hydrostatic 'preconditioning' are analysed.

## 3 THEORETICAL BACKGROUND: VISCOELASTIC DAMAGE RHEOLOGY

We use a viscoelastic damage rheology model that quantitatively explains general aspects of brittle rock deformation. In this section, we present a short background with the main features of the model. For more details on the theoretical background and comparisons with rock mechanics experiments see Lyakhovsky & Myasnikov (1984,
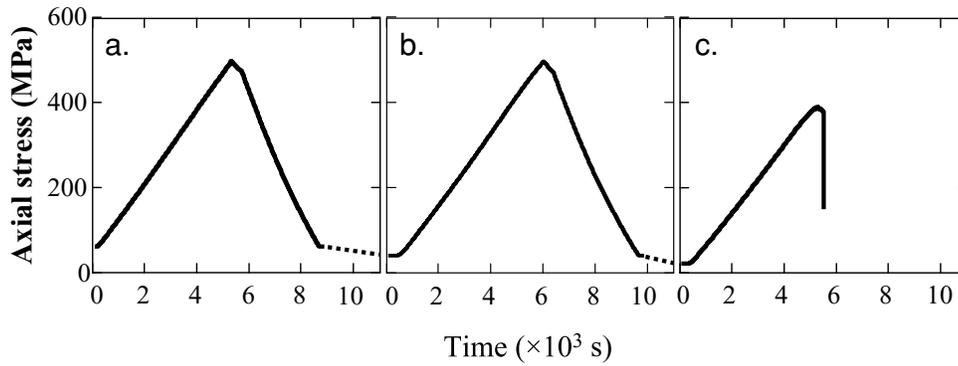
**Figure 1.** Loading histories during the three analysed deformation cycles. (a) First cycle is under 60 MPa confining pressure. (b) Second cycle is under 40 MPa confining pressure. (c) Third cycle is under 20 MPa confining pressure. The stress–drop during the last cycle signifies macroscopic brittle failure of the sample.

1985), Lyakhovsky *et al.* (1997a, 1997b), Agnon & Lyakhovsky (1995), Hamiel *et al.* (2004a, 2005, 2006), Ben-Zion & Lyakhovsky (2006) and Lyakhovsky & Ben-Zion (2008).

The effects of pre-existing cracks (i.e. constant damage) on the elastic properties of a solid are accounted for in the damage model by generalizing the strain energy to the form

$$U = \frac{1}{\rho}\left(\frac{\lambda}{2}I_1^2 + \mu I_2 - \gamma I_1\sqrt{I_2}\right), \tag{1}$$

where $I_1 = \varepsilon_{ii}$ and $I_2 = \varepsilon_{ij}\varepsilon_{ij}$ (Einstein's summation convention is assumed) are the first and second invariants of the elastic strain tensor $\varepsilon_{ij}$, $\rho$ is the mass density, $\lambda$ and $\mu$ are the Lamé parameters and $\gamma$ is a third modulus of a damaged solid. The first two terms of the energy potential (1) give the classical strain potential of linear elasticity. The third term may be derived using the effective medium theory of Budiansky & O'Connell (1976) for non-interacting cracks that dilate and contract in response to tension and compression (Lyakhovsky *et al.* 1997b), or by expanding the strain energy potential as a general second-order function of $I_1$ and $I_2$ and eliminating non-physical terms (Ben-Zion & Lyakhovsky 2006). Differentiation of the elastic energy (1) with respect to the strain tensor $\varepsilon_{ij}$ leads to a constitutive stress–strain relation given by

$$\sigma_{ij} = \rho\frac{\partial U}{\partial \varepsilon_{ij}} = \left(\lambda - \frac{\gamma}{\xi}\right)I_1\delta_{ij} + 2\left(\mu - \frac{1}{2}\gamma\xi\right)\varepsilon_{ij}, \tag{2}$$

where $\delta_{ij}$ is Kronecker delta and $\xi = I_1/\sqrt{I_2}$ is a strain invariant ratio ranging from $\xi = -\sqrt{3}$ for isotropic compaction to $\xi = \sqrt{3}$ for isotropic dilation. Eq. (2) reduces to linear Hookean elasticity for an undamaged solid ($\gamma = 0$), whereas distributed microcracks and flaws associated with $\gamma > 0$ leads to reduction of the effective elastic moduli and non-linear elasticity with asymmetric response to loading under tension and compression conditions. Eq. 2 can be expressed through the dependence of the effective elastic moduli ($\lambda^e = \lambda - \gamma/\xi$; $\mu^e = \mu - \gamma\xi/2$) on the strain invariant ratio and their abrupt change with transition from compacting ($\xi < 0$) to dilating ($\xi > 0$) strains. Change in the effective elastic moduli under stress reversal in a four-point beam test (Weinberger *et al.* 1994) for rock dilation due to deviatoric stresses (Hamiel *et al.* 2005) and in other rock mechanics experiments (Lyakhovsky *et al.* 1993, 1997b) confirm the applicability of the non-linear stress–strain relations (2) derived from the potential (1).

The evolution of rock damage and effective elastic properties is achieved by introducing functional relations $\lambda(\alpha)$, $\mu(\alpha)$ and $\gamma(\alpha)$ between the elastic moduli and a scalar damage variable $\alpha$ representing the internal crack density. The damage variable $\alpha$ ranges

between 0 and 1, where in undamaged material $\alpha = 0$ and macroscopic brittle failure occurs at critical $\alpha$. Using the balance equations of energy and entropy and accounting for irreversible changes related to viscous deformation and material damage, the equation of damage evolution has the form (Lyakhovsky *et al.* 1997a)

$$\frac{d\alpha}{dt} = -C\frac{\partial U}{\partial \alpha}, \tag{3}$$

where $C$ is a positive function of state variables that ensures non-negative local entropy production. Eq. (3) can describe not only damage increase or material degradation but also the process of material recovery associated with healing of microcracks. The latter is favoured by high confining pressure, low shear stress and high temperature. In the context of the laboratory fracturing experiments discussed in this study, the healing process is not relevant.

Agnon & Lyakhovsky (1995) and Lyakhovsky *et al.* (1997a) analysed the connection between the elastic moduli and $\alpha$. They suggested constant $\lambda$ and the following linear approximations: $\mu = \mu_0 + \mu_1\alpha$, $\gamma = \gamma_1\alpha$, with $\mu_0$, $\mu_1$ and $\gamma_1$ constants for each material. Substituting (1) into (3), the damage evolution can be rewritten as

$$\frac{d\alpha}{dt} = C_d I_2 (\xi - \xi_0), \tag{4}$$

where $C_d > 0$ describes the rate of damage evolution for a given deformation and is constrained by the time span in rock mechanics experiments between the onset of AE and macroscopic sample failure. The threshold $\xi_0$ for positive damage evolution is a material property, controlling the transition from healing to degradation, and is related to the internal friction angle (Agnon & Lyakhovsky 1995).

Analysis of observed deformation and AE from laboratory experiments in granites and sandstones led Hamiel *et al.* (2004a) to incorporate in the model a gradual damage-related inelastic deformation before the occurrence of macroscopic brittle failure. This inelastic strain $\varepsilon_{ij}^v$ starts to accumulate with the onset of AE, and the rate of its accumulation is assumed to be proportional to the rate of damage increase:

$$\frac{d\varepsilon_{ij}^v}{dt} = \begin{cases} C_v \dfrac{d\alpha}{dt}\sigma_{ij}^d & \dfrac{d\alpha}{dt} > 0 \\ 0 & \dfrac{d\alpha}{dt} \leq 0 \end{cases}, \tag{5}$$

where $C_v$ is a material constant and $\sigma_{ij}^d$ is the deviatoric stress tensor. The inverse of viscosity ($C_v d\alpha/dt$) relates the deviatoric stress to the rate of irreversible strain accumulation. Following Maxwell viscoelastic rheology, the total strain tensor $\varepsilon_{ij}^{tot}$ is assumed to be a

sum of the elastic strain tensor and the irreversible viscous component of deformation, that is, $\varepsilon_{ij}^{\text{tot}} = \varepsilon_{ij} + \varepsilon_{ij}^{v}$. This model assumption means that the total irreversible strain accumulated during the loading should be proportional to the overall damage increase in the tested rock sample.

# 4  SEISMIC WAVE VELOCITIES

The elastic energy potential (1) is formulated in terms of strain invariants without explicitly introducing material anisotropy. However, the potential includes non-linear elastic response that produces local anisotropy in a damaged volume. A propagating small amplitude seismic wave in the non-linear elastic media is associated with perturbations of the pre-defined state of stress corresponding to the initial strain value $\varepsilon_{ij}^{(0)}$. The relation between the wave-related perturbations of stress $\sigma_{ij}^{(1)}$ and strain $\varepsilon_{ij}^{(1)}$, in the vicinity of this pre-defined state of stress, is obtained by linearization of the non-linear stress–strain relation (2):

$$\sigma_{ij}^{(1)} = \left( \lambda\delta_{nm} - \gamma\frac{\varepsilon_{nm}^{(0)}}{\sqrt{I_2^{(0)}}} \right)\delta_{ij}\varepsilon_{nm}^{(1)} + \left( 2\mu - \gamma\frac{I_1^{(0)}}{\sqrt{I_2^{(0)}}} \right)\delta_{in}\delta_{jm}\varepsilon_{nm}^{(1)}$$
$$- \gamma\left( \frac{\delta_{nm}}{\sqrt{I_2^{(0)}}} - \frac{I_1^{(0)}}{I_2^{(0)}\sqrt{I_2^{(0)}}}\varepsilon_{nm}^{(0)} \right)\varepsilon_{ij}^{(0)}\varepsilon_{nm}^{(1)}. \tag{6}$$

The stress–strain relations (6) are equivalent to the usual stress–strain relations for an anisotropic elastic medium $\sigma_{ij}^{(1)} = C_{ijnm}\varepsilon_{nm}^{(1)}$, with a fourth-rank tensor $C_{ijnm}$ of the strain-dependent effective elastic moduli:

$$C_{ijnm} = \left( \lambda\delta_{nm} - \gamma\frac{\varepsilon_{nm}^{(0)}}{\sqrt{I_2^{(0)}}} \right)\delta_{ij} + \left( 2\mu - \gamma\frac{I_1^{(0)}}{\sqrt{I_2^{(0)}}} \right)\delta_{in}\delta_{jm}$$
$$- \gamma\left( \frac{\delta_{nm}}{\sqrt{I_2^{(0)}}} - \frac{I_1^{(0)}}{I_2^{(0)}\sqrt{I_2^{(0)}}}\varepsilon_{nm}^{(0)} \right)\varepsilon_{ij}^{(0)}. \tag{7}$$

For hydrostatic loading, the effective elastic moduli (7) can be reduced to the ordinary Lamé constants or Young's modulus and Poisson's ratio of linear elasticity. However, under non-hydrostatic loading, stress- and damage-induced seismic wave anisotropy is expected due to crack opening in different stress-preferred orientations. General relations between the fourth-rank tensor of the elastic moduli $C_{ijnm}$ and seismic wave velocities may be found in e.g. Mavko *et al.* (1998) and Aki & Richards (2002). Here we use the special form of this tensor and re-derive the expressions for the seismic wave velocities. Following the standard practice for elastic waves (e.g. Ben-Zion 2003), we substitute the stress–strain relation (6) into the Cauchy equation of motion for a continuum solid:

$$\rho\frac{\partial^2 u_n}{\partial t^2} = \frac{\partial\sigma_{nj}}{\partial x_j}, \tag{8}$$

where $u_n$ is the wave-related displacement vector. For mathematical simplicity, we limit our following derivation to the case of wave propagation in the $x$-direction and will rotate the coordinate system to calculate wave velocity in an arbitrary direction. The displacement vector for a wave propagating with angular frequency $\omega$ and wavenumber vector $k_n = (1,0,0)$ is

$$u_n = A_n e^{i(k_1 x - \omega t)}. \tag{9}$$

Combining eqs (6), (8) and (9) lead to the Helmholtz equation relating the amplitude, angular frequency and wavenumber vector.

This equation can be reduced to the following system of three linear equations

$$A_n\left( \lambda k_n k_i + \mu^e k_n k_i - \gamma e_{ij} k_n k_j + \mu^e k_m k_m \delta_{in} \right.$$
$$\left. - \gamma e_{nm} k_m k_i + \gamma\xi e_{ij} e_{nm} k_m k_j - \rho\omega^2\delta_{in} \right) = 0, \tag{10a}$$

where $e_{ij} = \varepsilon_{ij}/\sqrt{I_2}$. This set of three eqs (10a) has non-trivial solutions only for vanishing determinant of the associated matrix

$$\det\left( \lambda k_n k_i + \mu^e k_n k_i - \gamma e_{ij} k_n k_j + \mu^e k_m k_m \delta_{in} \right.$$
$$\left. - \gamma e_{inm} k_m k_i + \gamma\xi e_{ij} e_{nm} k_m k_j - \rho\omega^2\delta_{in} \right) = 0. \tag{10b}$$

This condition is satisfied if the ratio $\omega^2/k^2 = V^2$ is one of the three eigenvalues of the matrix of (10a). Therefore, three different types of waves exist in anisotropic media, instead of the two standard $P$ and $S$ types of waves of isotropic solid. These three types are referred to (e.g. Mavko *et al.* 1998; Aki & Richards 2002; Schubnel & Gueguen 2003) as quasi-longitudial, quasi-shear and pure shear. Similarly to the general case discussed by Mavko *et al.* (1998) and Schubnel & Gueguen (2003), the first eigenvalue

$$V_s^2 = \frac{\mu^e}{\rho}, \tag{11}$$

corresponds to a pure shear and isotropic wave, with velocity calculated using the effective shear modulus $\mu^e$. Using the solution (11) for the first eigenvalue, the equation for the second and third eigenvalues reduces to the quadratic equation

$$F^2 - F\left( \lambda + \mu^e - 2\gamma e_{11} + \gamma\xi(e_{11}^2 + e_{12}^2 + e_{13}^2) \right)$$
$$+ \left[ (\lambda + \mu^e)\gamma\xi - \gamma^2 \right]\left( e_{12}^2 + e_{13}^2 \right) = 0, \tag{12}$$

where $F = \rho V^2 - \mu^e$. The roots for eq. (12) correspond to the two different additional wave velocities of the examined anisotropic solid. One for the compressional (or quasi-longitudinal) wave, with velocity $V_P$, is given by

$$V_P^2 = \frac{\mu^e + \frac{1}{2}A + \sqrt{\frac{A^2}{4} - B}}{\rho}, \tag{13}$$

and another type of quasi-shear wave $V_{qS}$ is given by

$$V_{qS}^2 = \frac{\mu^e + \frac{1}{2}A - \sqrt{\frac{A^2}{4} - B}}{\rho}, \tag{14}$$

where the coefficients $A$ and $B$ are

$$A = \lambda + \mu^e - 2\gamma e_{11} + \gamma\xi\left( e_{11}^2 + e_{12}^2 + e_{13}^2 \right)$$
$$B = \left[ (\lambda + \mu^e)\gamma\xi - \gamma^2 \right]\left( e_{12}^2 + e_{13}^2 \right). \tag{15}$$

Note that in the case of $\gamma = 0$, that is, damage-free intact rock, the stress–strain relations reduce to Hookean elasticity and the wave velocities become the well-known expressions from linear elasticity

$$V_S^2 = V_{qS}^2 = \frac{\mu_0}{\rho},$$
$$V_P^2 = \frac{\lambda + 2\mu_0}{\rho}. \tag{16}$$

Eqs (13) and (14) predict that the seismic wave velocities $V_P$ and $V_{qS}$ become anisotropic for a solid with pre-existing damage ($\alpha > 0$) under non-hydrostatic load. Fig. 2 demonstrates these velocities in the polar coordinate system. The anisotropy in Fig. 2 is induced by uniaxial loading (the polar angle $\phi = 0°$ or $180°$ is the loading direction) applied to a material with initial Lamé parameters values of $\lambda_0 = 16$ GPa and $\mu_0 = 33$ GPa. These values are appropriate
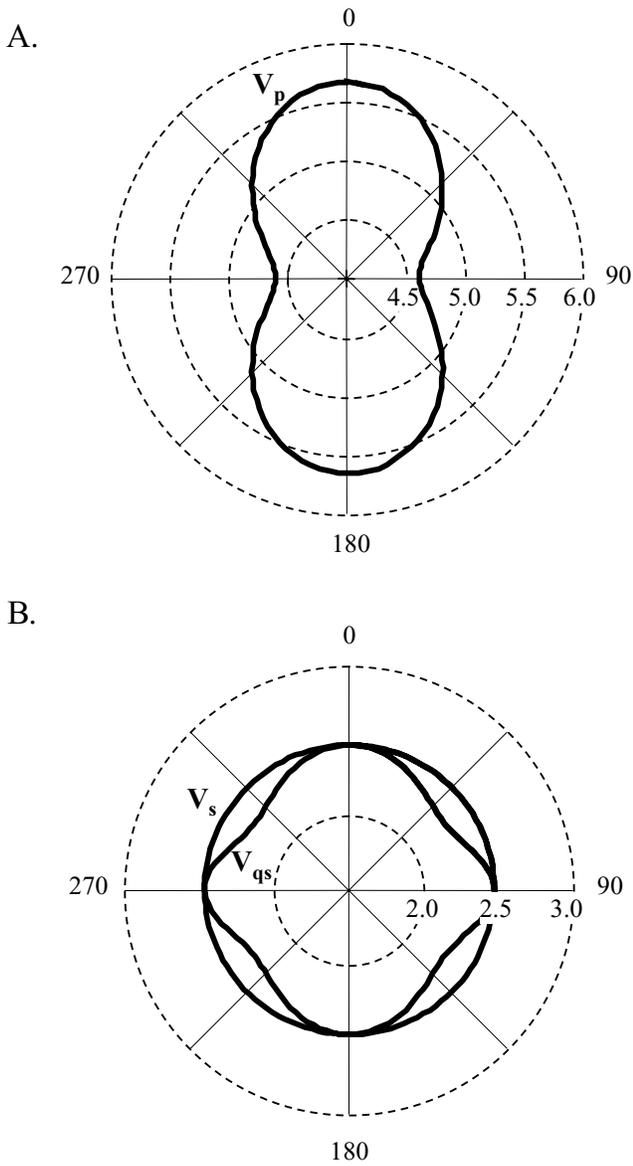
**Figure 2.** Model predicted azimuth dependence of wave velocities. (a) Results for $V_P$ corresponding to the quasi-longitudinal wave. (b) Results for $V_{qS}$ and $V_S$ corresponding to the quasi-shear and pure shear waves, respectively. The loading is uniaxial, $0°/180°$ corresponds to the directions along the axis of the loading and $90°/270°$ correspond to transverse directions.

for the Aue granite samples used in the laboratory experiments, analysed in the next section. The effective elastic moduli were calculated assuming a material damage of $\alpha = 0.3$, which is similar to the value characterizing the beginning of the third cycle of the examined deformation. With these parameters, a maximum value of about $V_P = 5.7$ km s$^{-1}$ is obtained in the axial direction and a minimum value of about $V_P = 4.6$ km s$^{-1}$ is obtained perpendicular to this direction (Fig. 2a). The quasi-shear wave velocity $V_{qS}$ in the axial and transversal directions is equal to the pure shear velocity $V_S$. The minimum $V_{qS}$ values are predicted along two orientations (four directions) that are oblique to the loading (Fig. 2b). In the next section, we compare laboratory results with the predicted damage- and stress-induced anisotropy of $P$ waves, which are associated with microcracks opening and closure, depending on their orientation relative to the applied stress.
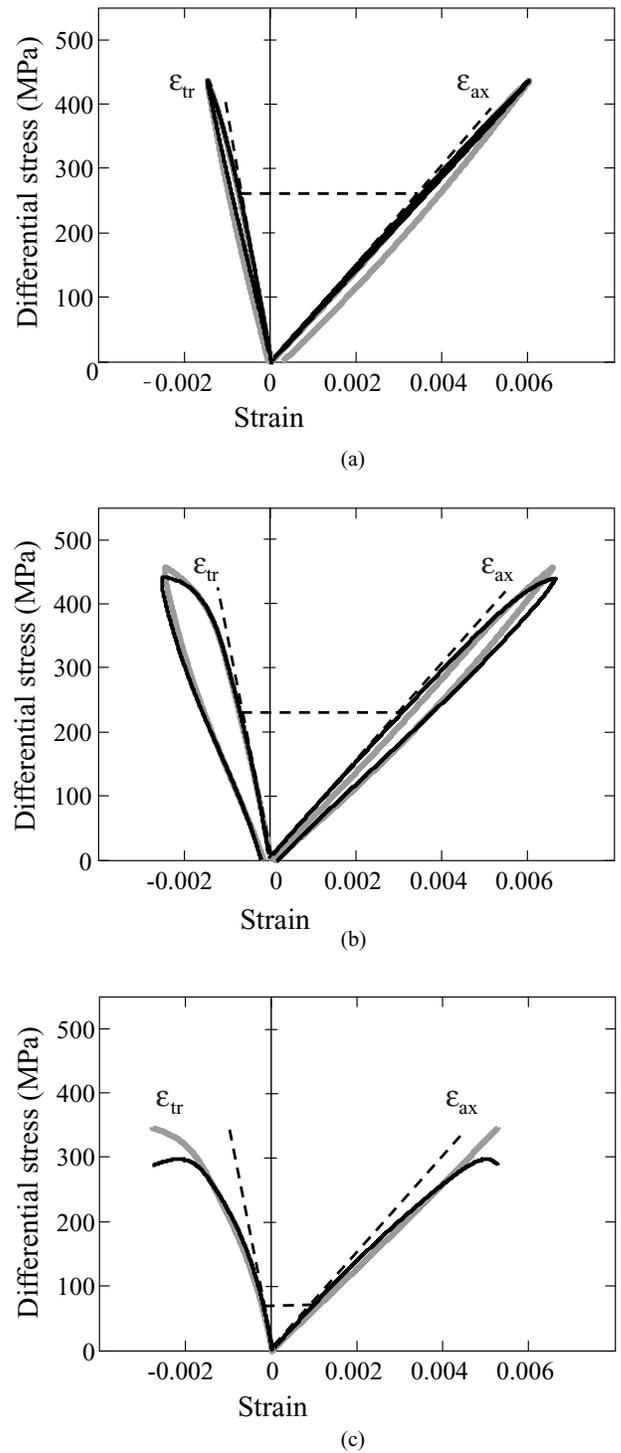
**Figure 3.** Comparison between measured (grey) and simulated (black) stress–strain relations in the three loading cycles. (a) First cycle is under 60 MPa confining pressure. (b) Second cycle is under 40 MPa confining pressure. (c) Third cycle is under 20 MPa confining pressure culminated by a macroscopic brittle failure.

## 5 ANALYSIS OF EXPERIMENTAL OBSERVATIONS

The continuous monitoring of axial and transversal strain components during cyclic triaxial compressional tests enables us to constrain the parameters of the damage rheology model. Fig. 3 shows
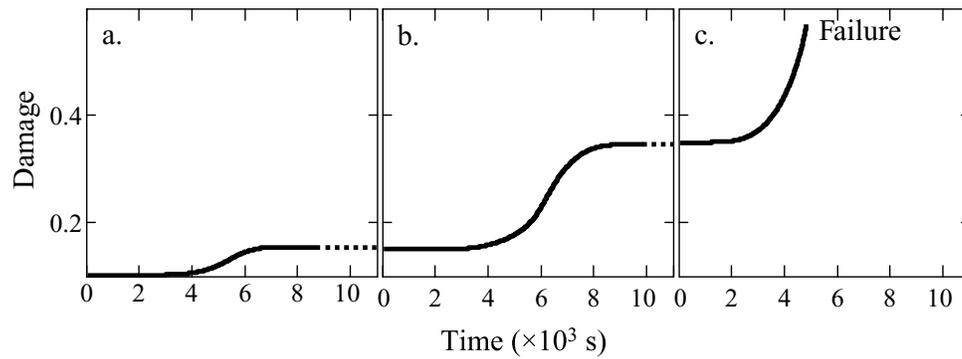
**Figure 4.** Model predicted damage accumulation during the three loading cycles.

the stress–strain relations for three loading cycles under 60, 40 and 20 MPa confining pressures and the simulated stress–strain curves. During the first cycle (Fig. 3a), the stress–strain relations for both axial and transversal components exhibit almost linear relations until approximately 260 MPa differential stress. At higher differential stresses, these relations deviate from linearity, especially for the transverse component. The point where the stress–strain curve departs from the initial linear relation corresponds to the onset of damage and provides an estimate from the measured strain components for the critical strain invariant ratio of $\xi_0 = -0.9$. Similar procedure was applied to the second and third deformation cycles (Figs 3b and c) and provided almost the same $\xi_0$ value. The linear part of the stress–strain curves from the first cycle is used to evaluate the elastic moduli of the initial Aue granite sample. Assuming a low pre-existing damage value of $\alpha = 0.1$, the Lamé constants for the damage-free material are $\lambda = 1.6 \times 10^4$ MPa, $\mu_0 = 3.3 \times 10^4$ MPa.

Two coupled processes, damage increase and the related gradual accumulation of inelastic strain lead to deviation of the stress–strain curve from the initial linear path. The rate of damage increase is controlled by the kinetic coefficient $C_d$, while the damage-related viscosity is controlled by the value of the coefficient $C_v$. A purely elastic damage rheology model with $C_v = 0$ can reproduce well the stress–strain curve during the loading part of the cycle, but it does not account for the inelastic accumulated strain during the whole cycle (e.g. Hamiel *et al.* 2004a). This inelastic component was clearly observed during the second cycle (Fig. 3b). To reduce the uncertainty in the evaluation of the damage model coefficients, we start the analysis using the elastic damage rheology with $C_v = 0$ and search for the value of the kinetic coefficient $C_d$, using only the loading part of the cycles. After constraining the $C_d$ value from fitting the loading parts, the damage-related viscosity terms (5) of

the viscoelastic model are included in analysis of the entire experimental stress–strains cycles. This approach gives rise to improved fitting of the unloading paths with minor changes of the loading paths. Following this approach, we obtain for the Aue granite samples the coefficients values of $C_v = 5 \times 10^{-6}$ MPa$^{-1}$ and $C_d = 3$ s$^{-1}$. The above single set of the model coefficients produces good quantitative agreement between the experimental and calculated stress–strain curves for all three cycles, except the latest stage prior to the strong damage localization and macroscopic failure at the end of the third cycle. The damage increase during the first and second cycles is relatively minor (Figs 4a and b) and the whole sample may be analysed in terms of uniform deformation. Toward the macroscopic brittle failure of the sample in the third cycle, the damage rapidly increases (Fig. 4c) and tends to localize into a narrow fault zone (e.g. Lockner *et al.* 1992; Hamiel *et al.* 2004a). Modelling detailed evolution of the damage prior to failure requires full 3-D numerical simulations that account for the strong spatial variability that develops at that stage. Such 3-D modelling was presented by Hamiel *et al.* (2004a); however, it is beyond the scope of the presented study.

The damage rheology model predicts different *P*-wave velocities in the axial (vertical) and transversal (horizontal) directions. The predicted velocity values were calculated using the set of model parameters constrained above by the measured stress–strain relations and compared with the experimentally measured velocities (Fig. 5). Relatively small anisotropy values were predicted by the model and experimentally observed during the first loading cycle under 60 MPa confining pressure (Fig. 5a). The small damage generated in that cycle (Fig. 4a), along with the relatively high confining pressure lead to an almost isotropic behaviour. More significant anisotropy is predicted and observed during the initial part of the second cycle
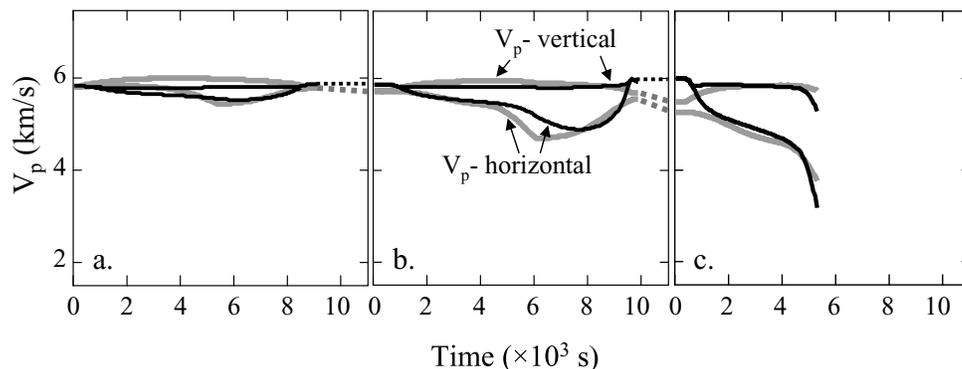


**Figure 5.** Comparison between measured (grey) and simulated (black) horizontal and vertical *P*-wave velocity in the three examined loading cycles.

(Fig. 5b). The anisotropy is strongly enhanced with the high damage increase after ∼4000 s from the beginning of the second cycle. The small discrepancy between the observed and simulated wave velocities at the end of the third cycle may be related to the strong damage localization at the final stages of damage evolution. This localization is a common feature of granite sample fracturing (e.g. Lockner *et al.* 1992) and requires 3-D calculations that account for heterogeneity of damage distribution (Hamiel *et al.* 2004a). The employed model accounts for the material weakening as well as damage- and stress-induced anisotropy under non-hydrostatic load, but it ignores small changes in the *P*-wave velocity associated with the reduction of the confining pressure. This effect, discussed by Stanchits *et al.* (2006) for granite and basalt samples, produces pressure-induced *P*-wave velocity change at low confining pressures. This pressure dependence leads to a certain reduction of the *P*-wave velocity between the end of the second cycle (40 MPa) and beginning of the third cycle (20 MPa) and produces some discrepancies between the model predictions and observations (Figs 5b and c) under low pressures. However, with the increase of the differential load during the third cycle, the pressure effect becomes negligible and the model-predicted velocities fit well the observations, including the strong velocity reduction prior to the final macroscopic failure (Fig. 5c).

## 6 DISCUSSION

We present theoretical results of a non-linear damage rheology for brittle rock deformation in relation to laboratory observations obtained in fracturing experiments of granite. The examined quantities include evolving stress–strain relations and anisotropy of elastic waves induced by material damage and stress during several deformation cycles (Fig. 1). A linearization of a non-linear stress–strain relation (eq. 2) in the vicinity of this pre-defined state of stress leads to connections (eq. 6) between small wave-related perturbations of the stress and strain fields. These relations have a tensorial structure with a forth-rank tensor of the effective elastic moduli depending explicitly on the pre-existing load. Analytical expressions for the associated elastic waves have propagation velocities that depend on the load and the level of material damage.

Propagation of seismic waves in linear anisotropic elastic media has been studied extensively in the past (e.g. Mavko *et al.* 1998). In the general linear anisotropic case, three different types of elastic waves—quasi-longitudinal, quasi-shear and pure shear—with different velocities that depend on the direction of the wave propagation are expected (e.g. Aki & Richards 2002; Schubnel & Gueguen 2003). Due to the specific structure of the tensor of elastic moduli in the employed damage model, the pure shear wave in the obtained results is isotropic. The velocities of the other two waves strongly depend on the direction of wave propagation (Fig. 2).

The pure shear wave becomes anisotropic in a damage model with tensorial damage variable based on a crack-density tensor (e.g. Kachanov 1980, 1992; Sayers & Kachanov 1991). Such tensorial damage models are associated with two tensors of material properties; one is a second-rank and the other being fourth-rank tensor, related to the normal and tangential crack compliances. Sayers (2002) suggested a procedure based on six independent measurements of the *S*-wave velocity ($V_{12}$, $V_{21}$, $V_{13}$, $V_{31}$, $V_{23}$, $V_{32}$) and three measurements of the *P*-wave velocity ($V_{11}$, $V_{22}$, $V_{33}$) to invert observations for the crack density and the effective elastic properties of the damaged material. Hall *et al.* (2008) modified this procedure and suggested a new mathematical algorithm for the crack density tensor inversion, based on a limited number of measured veloci-

ties. Although these procedures can be used to estimate the crack density tensor for a given material state, they do not account for evolutionary processes leading to changes in the crack population. The damage model used in this work is associated with a scalar isotropic damage variable, but the non-linearity of the stress–strain relations stemming from the employed generalized elastic potential leads to the emergence of wave anisotropy. In addition, the model accounts for the evolution of material damage during deformation that exceeds the purely elastic regime. Laboratory results indicate that there is a significant difference between the values of elastic moduli calculated from wave velocities and from the stress–strain curve measured during the same experiment (see, e.g. fig. 9 in Stanchits *et al.* 2006). These discrepancies are ignored by the linear tensorial damage rheology models but accounted for by the non-linear scalar damage model employed in this paper.

Using the results of the first deformation cycle in the laboratory experiment, we constrain the parameters of the damage model that are appropriate for the Aue granite. Using the same set of parameters, we are able to fit the overall features of the second and third deformation cycles almost up to the final macroscopic failure. The calculated *P*-wave velocities and stress- and damage-induced anisotropy, using the model parameters constrained by the stress–strain relation, fit well the measured velocity values. Thus, the employed damage model accounts quantitatively for the overall aspects of the stress–strain fields beyond linear elasticity, while simultaneously reproducing the main features of the damage- and stress-induced elastic wave anisotropy measured during the experiments.

The employed model ignores small changes in the *P*-wave velocity associated with reduction of the confining pressure (e.g. Stanchits *et al.* 2006). For low porosity rocks like granite, the pressure-induced *P*-wave velocity change is relatively small, but for high porosity rocks like basalt or porous sandstone this effect can be much more significant. Stanchits *et al.* (2006) explained this effect previously, using the model of Soga *et al.* (1978) with penny-shape cracks having planes oriented parallel and perpendicular to the compression direction. In this model, a slight increase of the axial *P* velocity right after the application of axial load is related to the closure of horizontally oriented cracks, and the appearance of stress-induced anisotropy (accompanied by a significant decrease of the transverse *P* velocity) is related to the opening of vertically oriented cracks. A modified version of the damage rheology model that accounts for the evolution of both cracks and porosity of the type used by Hamiel *et al.* (2004b) may be used to model the pressure-induced *P*-wave velocity changes. This effect exists only for relatively low confining pressures and disappears for pressures of the order of tens MPa, corresponding to depths of the seismogenic zone. Nevertheless, it is important to account for this effect since recorded seismic data are strongly affected by the properties of the shallow crust where the confining pressure is low (e.g. Peng & Ben-Zion 2004; Liu *et al.* 2005; Boness & Zoback 2006). Our continuing work will focus on adding the pressure-induced *P*-wave velocity changes to the analysis of the laboratory data and using 3-D numerical simulations to model additional aspects of the results that depend strongly on spatial variations within the laboratory samples.

# REFERENCES

Agnon, A. & Lyakhovsky, V., 1995. Damage distribution and localization during dyke intrusion, in *The Physics and Chemistry of Dykes,* pp. 65–78, eds Baer, G. & Heimann, A., Balkema, Rotterdam.

Aki, K. & Richards, P.G., 2002. *Quantitative Seismology,* 2nd edn, University Science Books, Sausalito.

Ben-Zion, Y., 2003. Appendix 2, Key Formulas in Earthquake Seismology, in *International Handbook of Earthquake and Engineering Seismology,* Part B, pp. 1857–1875, eds Lee, W. HK , Kanamori, H., Jennings, P. C. & Kisslinger, C., Academic Press, Boston.

Ben-Zion, Y. & Lyakhovsky, V., 2006. Analysis of aftershocks in a lithospheric model with seismogenic zone governed by damage rheology, *Geophys. J. Int.,* **165,** 197–210, doi:10.1111/j.1365–246X.2006.02878.x.

Bonner, B.P., 1974. Shear wave birefringence in dilating granite, *Geophys. Res. Lett.,* **1,** 217–220.

Boness, N.L. & Zoback, M.D., 2006. Mapping stress and structurally-controlled crustal shear velocity anisotropy in California, *Geology,* **34,** 825–828.

Budiansky, B. & O'Connell, R.J., 1976. Elastic moduli of a cracked solid, *Int. J. Solids Struct.,* **12,** 81–97.

Chaboche, J.-L., 1988. Continuum damage mechanics, *J. appl. Mech. ASME,* **55,** 59–72.

Chapman, M., 2003. Frequency-dependent anisotropy due to meso scale fractures in the presence of equant porosity, *Geophys. Prospect.,* **51,** 369–379.

Christensen, R.M., 1979. *Mechanical of Composite Materials,* Wiley-interscience, New York.

Crampin, S., 1987. Geological and industrial applications of extensive dilatancy anisotropy, *Nature,* **328,** 491–496.

Eshelby, J.D., 1957. The determination of the elastic field of an ellipsoidal inclusion and related problems, *Proc. R. Soc. Lond., A,* **241,** 376–396.

Hall, S.A., Kendall, J.M., Maddock, J. & Fisher, Q., 2008. Crack density tensor inversion for analysis of changes in rock frame architecture, *Geophys. J. Int.,* **173,** 577–592.

Hamiel, Y., Liu, Y., Lyakhovsky, V., Ben-Zion, Y. & Lockner, D., 2004a. A visco-elastic damage model with applications to stable and unstable fracturing, *Geophys. J. Int.,* **159,** 1155–1165.

Hamiel, Y., Lyakhovsky, V. & Agnon, A., 2004b. Coupled evolution of damage and porosity in poroelastic media: theory and applications to deformation of porous rocks, *Geophys. J. Int.,* **156,** 701–713.

Hamiel, Y., Lyakhovsky, V. & Agnon, A., 2005. Rock dilation, nonlinear deformation, and pore pressure change under shear, *Earth planet. Sci. Lett.,* **237,** 577–589.

Hamiel, Y., Katz, O., Lyakhovsky, V., Reches, Z. & Fialko Y., 2006. Stable and unstable damage evolution in rocks with implications to fracturing of granite, *Geophys. J. Int.,* **167,** 1005–1016.

Hansen, N.R. & Schreyer, H.L., 1994. A thermodynamically consistent framework for theories of elastoplasticity coupled with damage, *Int. J. Solids Struct.,* **31,** 359–389.

Hudson, J.A., 1981. Wave speeds and attenuation of elastic waves in material containing cracks, *Geophys. J. R. astr. Soc.,* **64,** 133–150.

Jaeger, J.C. & Cook, N.G.W., 1979. *Fundamentals of Rock Mechanics,* Chapman and Hall.

Ju, J.W., 1990. Isotropic and anisotropic damage variables in continuum damage mechanics, *J. Eng. Mech.,* **116,** 2764–2770.

Kachanov, M., 1980. Continuum model of medium with cracks, *J. Eng. Mech. ASCE,* **106,** 1039–1051.

Kachanov, L.M., 1986. *Introduction to Continuum Damage Mechanics,* Martinus Nijhoff Publishers, Dordrecht, pp. 135.

Kachanov, M., 1992. Effective elastic properties of cracked solids; critical review of some basic concepts, *Appl. Mech. Rev.,* **45,** 304–335.

Kachanov, M., 1994. On the concept of damage in creep and in the brittle-elastic range, *Int. J. Damage Mech.,* **3,** 329–337.

Leary, P.C., Crampin, S. & McEvilly, T.V., 1990. Seismic fracture anisotropy in the Earth's crust: an overview, *J. geophys. Res.,* **95,** 11 105–11 114.

Lemaitre, J., 1996. *A Course on Damage Mechanics,* Springer-Verlag, Berlin.

Liu, Y., Teng, T.L. & Ben-Zion, Y., 2005. Near-surface seismic anisotropy, attenuation and dispersion in the aftershock region of the 1999 Chi-Chi earthquake, *Geophys. J. Int.,* **160**(2), 695–706.

Lockner, D.A. & Byerlee, J.D., 1980. Development of fracture planes during creep in granite, in *Proceedings of the 2nd Conference on Acoustic Emission/Microseismic Activity in Geological Structures and Materials,* pp. 11–25, eds Hardy, H.R. & Leighton, F.W., Trans-Tech. Publications, Clausthal-Zellerfeld, Germany.

Lockner, D.A., Walsh, J.B. & Byerlee, J.D., 1977. Changes in seismic velocity and attenuation during deformation of granite, *J. geophys. Res.,* **82,** 5374–5378.

Lockner, D.A., Byerlee, J.D., Kuksenko, V., Ponomarev, A. & Sidorin, A., 1992. Observations of quasi-static fault growth from acoustic emissions, in *Fault Mechanics and Transport Properties of Rocks, International Geophysics Series,* **Vol. 51,** 3–31, eds Evans, B. & Wong, T.-F., Academic Press, San Diego, CA.

Lyakhovsky, V. & Ben-Zion, Y., 2008. Scaling relations of earthquakes and aseismic deformation in a damage rheology model, *Geophys. J. Int.,* **172,** 651–662, doi:10.1111/j.1365–246X.2007.03652.x.

Lyakhovsky, V. & Myasnikov V.P., 1984. On the behavior of elastic cracked solid, *Phys. Solid Earth,* **10,** 71–75.

Lyakhovsky, V. & Myasnikov, V.P., 1985. On the behavior of visco-elastic cracked solid, *Phys. Solid Earth,* **4,** 28–35.

Lyakhovsky, V. & Myasnikov, V. 1987. Relation between seismic wave velocity and state of stress, *Geophys. J. R. astr. Soc.,* **2,** 429–437.

Lyakhovsky, V. & Myasnikov, V. 1988. Acoustics of rheologically nonlinear solids, *Int. J. Phys. Earth Planet. Inter.,* **50,** 60–64.

Lyakhovsky, V., Podladchikov, Y. & Poliakov, A., 1993. Rheological model of a fractured solid, *Tectonophysics,* **226,** 187–198.

Lyakhovsky, V., Ben-Zion, Y. & Agnon, A., 1997a. Distributed damage, faulting, and friction, *J. geophys. Res.,* **102,** 27 635–27 649.

Lyakhovsky, V., Reches, Z., Weinberger., R. & Scott, T.E., 1997b. Non-linear elastic behaviour of damaged rocks, *Geophys. J. Int.,* **130,** 157–166.

Mavko, G., Mukerji, T. & Dvorkin, J., 1998. *The Rock Physics Handbook,* Cambridge University Press, New York, 329 pp.

Miller, V. & Savage, M.K., 2001. Changes in seismic anisotropy after volcanic eruptions: evidence from Mount Ruapehu, *Science,* **293,** 2231–2233.

Mogi, K., 1962. Study of the elastic shocks caused by the fracture of heterogeneous materials and its relation to earthquake phenomena, *Bull. Earthq. Res. Inst. Tokyo Univ.,* **40,** 125–173.

Myasnikov, V.P. & Topale, V.I., 1987. A seismically anisotropic lithosphere modeled by an elastic medium with different moduli, *Phys. Solid Earth,* **23,** 375–381.

Nur, A., 1971. Effects of stress on velocity anisotropy in rocks with cracks, *J. geophys. Res.,* **76,** 2022–2034.

Nur, A. & Simmons, G., 1969. Stress-induced velocity anisotropy in rock: an experimental study, *J. geophys. Res.,* **74,** 6667–6674.

O'Connell, R.J. & Budiansky, B., 1974. Seismic wave velocities in dry and saturated cracked solid, *J. geophys. Res.,* **79,** 5412–5426.

Peng, Z. & Ben-Zion, Y., 2004. Systematic analysis of crustal anisotropy along the Karadere-Düzce branch of the north Anatolian fault, *Geophys. J. Int.,* **159,** 253–274, doi:10.1111/j.1365–246X.2004.02379.x.

Rabotnov, Y.N., 1988. *Mechanics of Deformable Solids,* Science, Moscow, 712 pp.

Rathore, J.S., Fjaer, E., Holt, R.M. & Renlie, L., 1995. P- and S-wave anisotropy of a synthetic sandstone with controlled crack geometry, *Geophys. Prospect.,* **43,** 711–728.

Sammonds, P.R., Ayling, M.R., Meredith, P.G., Murrell, S.A.F. & Jones, C., 1989. A laboratory investigation of acoustic emission and elastic wave velocity changes during rock failure under triaxial stresses, in *Rock at*

*Great Depth,* pp. 233–240, eds Maury, V. & Fourmaintraux, D., A.A. Balkema, Rotterdam.

Sayers, C., 2002. Stress-dependent elastic anisotropy of sandstones, *Geophys. Prospect.,* **50,** 85–95.

Sayers, C. & Kachanov, M., 1991. A simple technique for funding effective elastic constants of cracked solids for arbitrary crack orientation statistics, *Int. J. Solids Struct.,* **27,** 671–680.

Sayers, C. & Kachanov, M., 1995. Microcrack-induced elastic wave anisotropy of brittle rocks, *J. geophys. Res.,* **100,** 4149–4156.

Sayers, C.M., Van Munster, J.G. & King, M.S., 1990. Stress-induced ultrasonic anisotropy in Berea sandstone, *Int. J. Rock Mech. Min. Sci. & Geomech. Abstr.,* **27,** 429–436.

Schoenberg, M. & Douma, J., 1988. Elastic wave propagation in media with parallel fractures and aligned cracks, *Geophys. Prospect.,* **36,** 571–589.

Schoenberg, M. & Sayers, C.M., 1995, Seismic anisotropy of fractured rock, *Geophysics,* **60,** 204–211.

Schubnel, A. & Guéguen, Y., 2003. Dispersion and anisotropy of elastic waves in cracked rocks, *J. geophys. Res.,* **108,** 2101, doi:10.1029/2002JB001824.

Soga, N., Mizutani, H., Spetzler, H. & Martin, R., 1978. The effect of dilatancy on velocity anisotropy in Westerly granite, *J. geophys. Res.,* **83,** 4451–4458.

Stanchits, S., Vinciguerra, S. & Dresen, G., 2006. Ultrasonic velocities, acoustic emission characteristics and crack damage of basalt and granite, *Pure appl. Geophys.,* **163,** 975–994.

Verdon, J.P, Angus, D.A, Kendall, J.M. & Hall, S.A., 2008. The effect of microstructure and nonlinear stress on anisotropic seismic velocities, *Geophysics,* **73,** D41–D51.

Weinberger, R., Reches, Z., Eidelman, A. & Scott, T.S., 1994. Tensile properties of rocks in four-point beam tests under confining pressure, in *Proceedings of the first North American Rock Mechanics Symposium,* pp. 435–442, eds Nelson, P. & Laubach, S.E., A.A. Balkema, Rotterdam.

Zamora, M. & Poirier, J.P., 1990. Experimental study of acoustic anisotropy and birefringence in dry and saturated Fontainebleau sandstone, *Geophysics,* **55,** 1455–1465.

Zang, A., Wagner, F., Stanchits, S., Janssen, C. & Dresen, G., 2000. Fracture process zone in granite, *J. geophys. Res.,* **105,** 23 651–23 661.